Chinese Journal of Natural Medicines

Emd-D inhibited ovarian cancer progression *via* PFKFB4-dependent glycolysis and apoptosis

Xin Zhao, Chao Chen, Xuefei Feng, Haoqi Lei, Lingling Qi, Hongxia Zhang, Haiying Xu, Jufeng Wan, Yan Zhang, Baofeng Yang

Citation: Xin Zhao, Chao Chen, Xuefei Feng, Haoqi Lei, Lingling Qi, Hongxia Zhang, Haiying Xu, Jufeng Wan, Yan Zhang, Baofeng Yang, Emd-D inhibited ovarian cancer progression *via* PFKFB4-dependent glycolysis and apoptosis, Chinese Journal of Natural Medicines, 2025, 23(4), 431-442. doi: 10.1016/S1875-5364(25)60843-0.

View online: https://doi.org/10.1016/S1875-5364(25)60843-0

Related articles that may interest you

Jiedu Sangen decoction inhibits chemoresistance to 5-fluorouracil of colorectal cancer cells by suppressing glycolysis *via* PI3K/AKT/HIF-1 α signaling pathway

Chinese Journal of Natural Medicines. 2021, 19(2), 143-152 https://doi.org/10.1016/S1875-5364(21)60015-8

Hernandezine promotes cancer cell apoptosis and disrupts the lysosomal acidic environment and cathepsin D maturation

Chinese Journal of Natural Medicines. 2024, 22(5), 387-401 https://doi.org/10.1016/S1875-5364(24)60638-2

Polygalacin D inhibits the growth of hepatocellular carcinoma cells through BNIP3L-mediated mitophagy and endogenous apoptosis pathways

Chinese Journal of Natural Medicines. 2023, 21(5), 346-358 https://doi.org/10.1016/S1875-5364(23)60452-2

Effects of chitooligosaccharide-zinc on the ovarian function of mice with premature ovarian failure *via* the SESN2/NRF2 signaling pathway

Chinese Journal of Natural Medicines. 2021, 19(10), 721-731 https://doi.org/10.1016/S1875-5364(21)60084-5

Bavachin induces apoptosis in colorectal cancer cells through Gadd45a *via* the MAPK signaling pathway

Chinese Journal of Natural Medicines. 2023, 21(1), 36-46 https://doi.org/10.1016/S1875-5364(23)60383-8

Identification of Bulbocodin D and C as novel STAT3 inhibitors and their anticancer activities in lung cancer cells

Chinese Journal of Natural Medicines. 2023, 21(11), 842-851 https://doi.org/10.1016/S1875-5364(23)60521-7

Wechat

Chinese Journal of Natural Medicines 23 (2025) 431-442

Contents lists available at ScienceDirect

Chinese Journal of Natural Medicines

journal homepage: www.cjnmcpu.com/

Original article

Emd-D inhibited ovarian cancer progression *via* PFKFB4-dependent glycolysis and apoptosis

Xin Zhao[a,b,Δ], Chao Chen[a,Δ], Xuefei Feng[a], Haoqi Lei[a], Lingling Qi[a], Hongxia Zhang[a], Haiying Xu[a], Jufeng Wan[a], Yan Zhang[a,b,*], Baofeng Yang[a,b,c,*]

[a] *Department of Pharmacology (State-Province Key Laboratories of Biomedicine-Pharmaceutics of China, Key Laboratory of Cardiovascular Medicine Research, Ministry of Education), College of Pharmacy, Harbin Medical University, Harbin 150081, China*

[b] *National Key Laboratory of Frigid Zone Cardiovascular Diseases (NKLFZCD), Harbin Medical University, Harbin 150081, China*

[c] *Research Unit of Noninfectious Chronic Diseases in Frigid Zone (2019RU070), Chinese Academy of Medical Sciences, Harbin 150081, China*

ARTICLE INFO

Article history:
Received 23 December 2023
Revised 11 April 2024
Accepted 27 April 2024
Available online 20 April 2025

Keywords:
Ovarian cancer
Emd-D
Glycolysis
Apoptosis
PFKFB4

ABSTRACT

Ovarian cancer poses a significant threat to women's health, necessitating effective therapeutic strategies. Emd-D, an emodin derivative, demonstrates enhanced pharmaceutical properties and bioavailability. In this study, Cell Counting Kit 8 (CCK8) assays and Ki-67 staining revealed dose-dependent inhibition of cell proliferation by Emd-D. Migration and invasion experiments confirmed its inhibitory effects on OVHM cells, while flow cytometry analysis demonstrated Emd-D-induced apoptosis. Mechanistic investigations elucidated that Emd-D functions as an inhibitor by directly binding to the glycolysis-related enzyme PFKFB4. This was corroborated by alterations in intracellular lactate and pyruvate levels, as well as glucose transporter 1 (GLUT1) and hexokinase 2 (HK2) expression. PFKFB4 overexpression experiments further supported the dependence of Emd-D on PFKFB4-mediated glycolysis and SRC3/mTORC1 pathway-associated apoptosis. *In vivo* experiments exhibited reduced xenograft tumor sizes upon Emd-D treatment, accompanied by suppressed glycolysis and increased expression of Bax/Bcl-2 apoptotic proteins within the tumors. In conclusion, our findings demonstrate Emd-D's potential as an anti-ovarian cancer agent through inhibition of the PFKFB4-dependent glycolysis pathway and induction of apoptosis. These results provide a foundation for further exploration of Emd-D as a promising drug candidate for ovarian cancer treatment.

1. Introduction

Ovarian cancer represents a significant gynecologic malignancy, accounting for a substantial portion of gynecologic tumor types [1, 2]. Epithelial ovarian cancer (EOC), which encompasses clear cell, mucinous, endometrial, low-grade plasmacytosis (LGS), and high-grade plasmacytosis (HGS) ovarian cancers, constitutes the most prevalent ovarian cancer subtype, comprising 50%–70% of cases [3]. The primary treatment for EOC involves surgical resection of the visible tumor mass, followed by administration of taxanes (paclitaxel, docetaxel, etc.) and/or platinum-based agents (cisplatin or carboplatin). Additionally, Bevacizumab has been incorporated into this standard chemotherapy regimen to improve progression-free survival (PFS) [4]. However, despite these interventions, approximately 60% of patients experience recurrence within six months or later due to refractory, chemoresistant tumors.

The primary energy source utilized by tumor cells originates from aerobic glycolysis, a metabolic pathway also referred to as the Warburg effect. During this process, cancer cells redirect a significant portion of pyruvate towards lactate production, circumventing entry into the tricarboxylic acid cycle necessary for complete oxidative phosphorylation. This alternative pathway provides dual advantages to cancer cells: it effectively inhibits the generation of reactive oxygen species (ROS), thereby protecting mitochondrial integrity, and it enables the maintenance of moderate ROS levels over extended periods, creating favorable conditions for tumor progression [5]. Consequently, targeting aerobic glycolysis in cancer cells represents a promising therapeutic strategy [6, 7]. Several pharmaceutical agents, including Lonidamine [8, 9] and 2-deoxy-D-glucose (2-DG) [10, 11], are currently under development to target glycolysis and impede tumor growth and metastasis. Notably, emodin has shown efficacy in suppressing glycolysis by modulating ROS levels [12]. However, the specific molecular target through which emodin exerts its effect remains to be elucidated.

Plant-derived compounds play a significant role in anti-tumor drugs [13]. Emodin, a natural anthraquinone compound, is widely found in *Rheum palmatum*, *Polygonum cuspidatum*, *Reyn-*

* Corresponding author.
E-mail addresses: zhangyan@ems.hrbmu.edu.cn (Y. Zhang); yangbf@ems.hrbmu.edu.cn (B. Yang)
Δ These authors contributed equally to this work.

https://doi.org/10.1016/S1875-5364(25)60843-0
Copyright © 2025, China Pharmaceutical University. Published by Elsevier B.V. All rights reserved.

outria multiflora, and other herbs. Previous studies have confirmed the inhibitory effects of Emodin on lung, liver and breast cancers [14-16]. However, its clinical application has been limited by adverse reactions such as diarrhea and hepatotoxicity [17-19]. Our research team has developed a novel derivative of emodin (Emd-D). The chemical structure is illustrated in Fig. 1A, which is anticipated to maintain the original pharmacological activities while mitigating adverse reactions. Preliminary research has demonstrated that Emd-D exhibits a lower Gibbs free energy than emodin, indicating a higher binding potential with target proteins and improved druggability [20]. Despite these advancements, the inhibitory effect of Emd-D on ovarian cancer and the underlying molecular mechanism remain unexplored, necessitating further investigation for confirmation.

This study investigated the anti-cancer potential of Emd-D, a newly synthesized derivative of emodin, against ovarian cancer. The results demonstrated that Emd-D significantly inhibited cell proliferation, migration, and invasion, while promoting apoptosis and inhibiting glycolysis both *in vitro* and *in vivo* using an ovarian cancer xenograft tumor model. Mechanistically, the research established that Emd-D exerts its anti-cancer effects by suppressing PFKFB4-dependent glycolysis and promoting apoptosis.

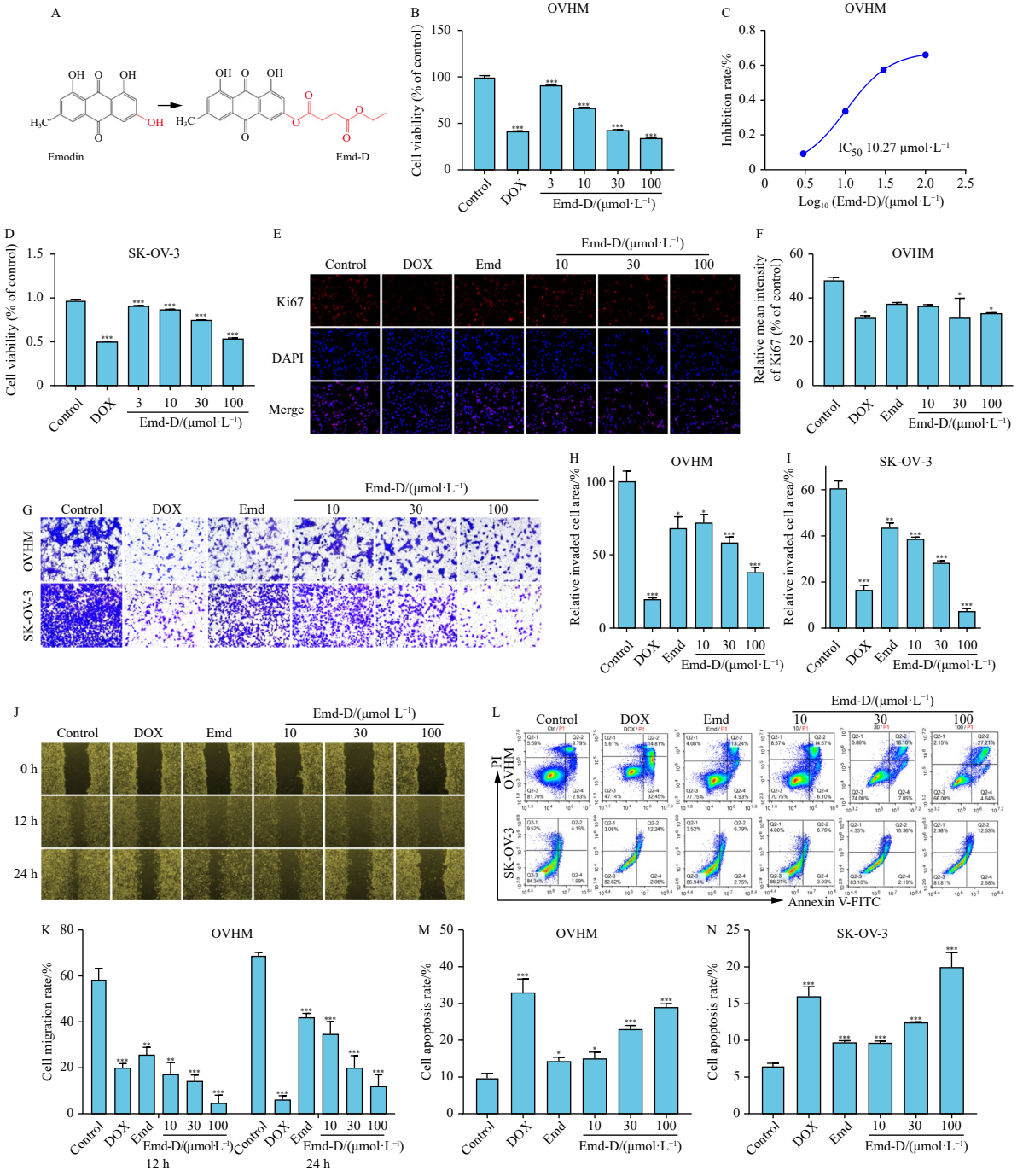

Fig. 1 Emd-D inhibits the proliferation, migration, and invasion of OVHM cells *in vitro*. (A) The structural formula of Emd-D. (B) Cell viability of OVHM cells treated with different concentration of Emd-D. (C) The IC_{50} value of 10.27 μmol·L^{-1} was calculated by Graphpad Prism software. (D) Cell viability of SK-OV-3 cells treated with different concentration of Emd-D. (E–F) Ki67 staining showing that Emd-D decreased the rate of Ki67-positive cells. (G–I) Transwell assay demonstrating the inhibitory effect of Emd-D on OVHM and SK-OV-3 cells invasion. (J–K) Wound healing assay demonstrating the inhibitory effect of Emd-D on OVHM cell migration aawszdxcfter 12 and 24 h. (L–N) Flow cytometry showing the Emd-D promoted apoptosis in a dose-dependent manner in OVHM and SK-OV-3 cells. All data are shown as the mean ± SEM (n = 4). $^{*}P$ < 0.05, $^{**}P$ < 0.01, and $^{***}P$ < 0.001 *vs* control.

2. Materials and Methods

2.1. Cell lines and regents

The OVHM and SK-OV-3 cell lines were obtained from Otwo Biotech and subsequently cultured in Dulbecco's Modified Eagle Medium (DMEM) (Hyclone, USA), supplemented with 10% fetal bovine serum (FBS) (Clark, USA) and 1% penicillin-streptomycin solution (Beyotime, China). The cells were maintained in a controlled environment at 37 °C, with 5% CO_2. For experimental purposes, Emd-D, a compound synthesized by the Science and Technology Park Laboratory of Pharmaceutical Chemistry at Harbin Medical University (Harbin, China), was initially dissolved in deionized water prior to its application.

2.2. Tumor xenograft model

Female BALB/C mice (specific pathogen-free grade, weighing 18 ± 2 g) were obtained from Liaoning Changsheng Biological Technology Co., Ltd. All experimental procedures received ethical approval from the Ethics Committee of Harbin Medical University. To establish the xenograft model, 3×10^5 tumor cells were subcutaneously injected into the right dorsal region of each mouse. The mice were subsequently randomized into five groups, each comprising 8 mice, and subjected to different treatments, including Doxorubicin (DOX) and Emd-D at doses of 20, 60, and 180 mg·kg^{-1}. DOX was administered intraperitoneally at 4 mg·kg^{-1} every 3 days, while Emd-D was orally administered daily. Tumor sizes were measured and recorded throughout the study using the formula: $V = L \times W2/2$, where V represents the tumor volume, L represents the length, and W represents the width of the tumor. After 21 d, the mice were euthanized, and the tumors were excised, weighed, and photographed for visual documentation.

2.3. Cell Counting Kit 8 (CCK8) assay

Cell viability was evaluated using the CCK8 assay. OVHM and SK-OV-3 cells were seeded in 96-well plates and subsequently exposed to varying concentrations of Emd-D (10, 30, 100 μmol·L^{-1}), emodin (10 μmol·L^{-1}), and DOX (10 μg·mL^{-1}). After a 24-h incubation period, the supernatant in each well was combined with 10 μL of CCK8 reagent (Solarbio, Beijing, China). The plates were incubated with the CCK8 reagent for 1 h in darkness. Following this, the plates were shaken on an oscillator for 10 min, and the absorbance of each well was measured at 450 nm using a microplate reader.

2.4. Cell transfection

OVHM cells were cultured in 6-well plates until reaching 70% to 90% confluence, followed by a 24-hour serum starvation period. The overexpression plasmid containing PFKFB4 cDNA was diluted in OPTI-MEM® I medium. LipofectamineTM 3000 liposomes and Opti-MEM® I were gently mixed to create a homogeneous solution. Subsequently, the diluted PFKFB4 cDNA and LipofectamineTM 3000 were combined and incubated at room temperature for 10-15 minutes. The resulting mixture was then added to the 6-well plate and incubated at 37 °C for 24–48 hours before analyzing the transfected cells.

2.5. Wound healing assay

OVHM cells were seeded in 6-well plates and cultured until reaching a confluence exceeding 90%. Following this, artificial wounds were created using a 10 μL pipette tip. The 6-well plates were subsequently washed with PBS, followed by the individual addition of emodin (10 μmol·L^{-1}) and Emd-D (10, 30, 100 μmol·L^{-1}). Cell migration was monitored and captured at 0, 12, and 24 h using an inverted microscope. Image Pro Plus software was employed to analyze the migration rate.

2.6. Transwell assay

The invasive capability of cells was evaluated using the Transwell assay. Transwell chambers (8.0 μm, Polycarbonate, Corning, USA) were pre-coated with Matrigel (Corning, USA). Approximately 5×10^4 cells were introduced into the upper chamber and exposed to varying concentrations of Emd-D (10, 30, 100 μmol·L^{-1}), emodin (10 μmol·L^{-1}), and DOX (10 mg·mL^{-1}). The lower chambers contained 500 μl of complete culture medium. Following incubation in a 5% CO_2 incubator at 37 °C for 24 h, the lower chambers were fixed with methanol for 20 minutes and stained with 0.1% crystal violet for 20 min. The stained cells were then examined under a light microscope.

2.7. Flow cytometry

Cell apoptosis was assessed using flow cytometry with double staining of fluorescein isothiocyanate (FITC)-labeled Annexin V (Annexin V-FITC) and propidium iodide (PI). The cells were trypsinized, washed twice with cold PBS, and then centrifuged to remove the supernatant. Subsequently, the cells were stained with the Flow Cytometry Apoptosis Detection Kit (4A Biotech, Beijing, China) and incubated for 15 min at room temperature in the dark. Finally, apoptotic cells were analyzed using a flow cytometer (Agilent, USA).

2.8. Quantitative real-time polymerase chain reaction (PCR)

The OVHM cells underwent treatment with 1 mL Trizol (Invitrogen, Boston, USA), followed by the addition of 200 μL chloroform to the cell lysate. The mixture was vigorously agitated for 20 sec, incubated on ice for 10 min, and then centrifuged at 4 °C and 13 500 r·min^{-1} for 15 min. The resulting aqueous phase was combined with an equal volume of isopropanol, gently mixed, and then incubated on ice for 10 min before being centrifuged at 4 °C and 13 500 r·min^{-1} for 15 min. Subsequently, the supernatant was discarded, and the precipitate was washed with 75% ethanol before being centrifuged at 4 °C and 10 600 r·min^{-1} for 15 min. The total RNA sample was dissolved in 20 μL DEPC water and reverse transcribed into cDNA using the Revert Aid First Strand cDNA synthesis kit (Thermo Scientific, Boston, USA). Finally, the cDNA samples underwent real-time PCR using FastStart Universal SYBR Green Master (ROX) (Roche, Basel, Switzerland) to determine the relative level of PFKFB4 mRNA.

2.9. Western blot analysis

Cell or tissue lysis was performed using RIPA buffer (Beyotime, Beijing, China) on ice to extract total proteins. These proteins were then separated through polyacrylamide gel electrophoresis and transferred onto an NC membrane (Millipore, MA, USA). Subsequently, the membranes were incubated overnight at 4 °C with primary antibodies. Following this, the membrane was washed with TBST buffer and incubated with horseradish peroxidase-conjugated anti-mouse or anti-rabbit secondary antibodies (1∶10 000, Li-CoR, Lincoln, USA) for 1 h. Finally, protein band intensity was analyzed by scanning the film using the Odyssey infrared fluorescence scanning imaging system and evaluating the gray value. Antibodies against β-actin were obtained from Bioss (Beijing, China), antibodies against

PFKFB4 were obtained from Abcam (Cambridge, UK), and antibodies against ATF-4, SRC-3, p-S6, S6, Bcl-2, and Bax were acquired from Cell Signaling Technology (Danvers, USA). Furthermore, antibodies against ASNS were sourced from Santa Cruz (Dallas, USA), antibodies against gluc- ose transporter 1 (GLUT1) and hexokinase 2 (HK2) were procured from Affinity (Wuhan, China), while antibodies against p-SRC-3 were obtained from Invitrogen (MA, USA). The experiment was replicated four times to ensure reliability.

2.10. Immunofluorescence staining

OVHM cells were cultured in 24-well plates and subsequently transfected. The culture medium was removed, and the cells were washed thrice with PBS for 5 minutes each. Following this, the cells were fixed in 4% paraformaldehyde for 30 minutes and permeabilized with 0.5% saponin (Beyotime, Shanghai, China) for 20 minutes. The fixed cells were then blocked with 5% BSA at room temperature for 45 minutes. Antibodies targeting PFKFB4, Ki67 and GLUT1 were incubated with the cells overnight at 4 °C. Finally, the cells were incubated with secondary antibodies (diluted 1∶100 in Immunol Fluoresce Staining Secondary Antibody Dilution Buffer, Beyotime) at room temperature for 1 hour and stained with DAPI for 4 minutes. Photomicrographs were captured using a fluorescence microscope.

2.11. Molecular docking

A molecular docking study was conducted to examine the binding mode between Emd-D and PFKFB4 utilizing Autodock Vina software 1.1.2 [21]. The three-dimensional structure of PFKFB4 (PDB ID: 1BIF) was obtained from the RCSB Protein Data Bank (www.rcsb.org). ChemBioDraw Ultra 14.0 was utilized to create the 2D structure of PFKFB4, which was subsequently converted to a 3D structure using ChemBio3D Ultra 14.0 software. The AutoDockTools 1.5.6 package [22, 23] was employed to generate the docking input files. In preparation for docking, the ligand was processed by merging non-polar hydrogen atoms and defining rotatable bonds. The search grid for the PFKFB4 binding site was defined with coordinates center_x: 49.332, center_y: 54.409, and center_z: 65.038 with dimensions size_x: 15, size_y: 15, and size_z: 15. To enhance docking accuracy, the exhaustiveness value was set to 16. For Vina docking, default parameters were utilized unless otherwise specified. The highest-scoring pose, as determined by the Vina docking score, was selected and subjected to visual analysis using PyMoL 1.7.6 software (www.pymol.org).

2.12. Drug Affinity Response Target Stability (DARTS) assay

Following the harvesting of OVHM cell lysates via centrifugation, protein concentrations were determined using the BCA protein kit. The extracted protein concentrations were then adjusted to 1.5 g·L^{-1} in M-PER buffer (Invitrogen, MA, USA). The protein solutions were subsequently incubated with DMSO or 30 μmol·L^{-1} Emd-D at room temperature for 2 h. Prior to further processing, the samples were pre-warmed on a metal bath at 40 °C for 10 min. Pronase E (Yuanye, Shanghai, China) PBS solution, with a concentration of 5 mg·mL^{-1} and an enzyme to protein ratio of 1∶50, was added to each sample group. The samples were immediately subjected to digestion on a metal bath at 40 °C for 20 min. Western blot analysis was then conducted to evaluate the expression of PFKFB4 protein.

2.13. Extracellular flux analysis

The Seahorse XP96 extracellular flow analyzer (Seahorse Bioscience) was utilized to measure the extracellular acidification rate (ECAR) following the manufacturer's recommended standard protocol. Specifically, OVHM and SK-OV-3 Cells underwent treatment with Emd-D at concentrations of 10, 30, and 100 μmol·L^{-1}, followed by a 24-hour incubation period. Subsequently, the cells were digested and 40 000 cells per well were seeded onto XF96 (V3) polystyrene cell culture plates. Before measurement, the original culture medium was replaced with XF culture medium, and the cells were equilibrated for 1 hour at 37 °C in a CO_2-free incubator. The sensor box was incubated in sterile water for 24 h, then refreshed with XF calibration solution for 1 h before assessing the ECAR of cells cultured in glucose-free medium. Glucose (10 mmol·L^{-1}) was introduced into the XF medium, followed by the addition of oligomycin (1 μmol·L^{-1}) and 2-deoxy-D-glucose (2-DG) (50 mmol·L^{-1}). Data collection and analysis were conducted using Seahorse XF Software, and statistical calculations were performed to determine the mean ± SEM.

2.14. Statistical analysis

In this study, data are presented as mean ± standard error (SEM). Statistical analysis and data processing were conducted using Graphpad Prism 8.0 software. For comparisons among multiple sets of data, Analysis of Variance (ANOVA) was employed, while the t -test was utilized for comparisons between two sets of data. Statistical significance was determined at a threshold of $P < 0.05$.

3. Results

3.1. Emd-D inhibited the proliferation and metastasis in vitro

To assess the effect of Emd-D on ovarian cancer cell viability, we exposed OVHM and SK-OV-3 cells to various concentrations (3, 10, 30, and 100 μmol·L^{-1}) of Emd-D for 24 h, and evaluated cell viability using the CCK8 assay. Our results indicate that Emd-D inhibits the proliferation of OVHM and SK-OV-3 cells in a dose-dependent manner, with an IC_{50} value of 10.27 μmol·L^{-1} for OVHM cells (Figs. 1B–1D). We also observed a significant reduction in the expression of Ki-67, a proliferation biomarker, following Emd-D treatment (Figs. 1E and 1F). Furthermore, as tumor metastasis is a critical factor in determining cancer cell malignancy, the effects of anti-tumor drugs on malignant cell migration and invasion should be thoroughly evaluated [24]. We assessed Emd-D's ability to suppress malignant cell migration and invasion using wound healing and Transwell assays. Our findings clearly demonstrate that Emd-D inhibits extracellular matrix traversal (Figs. 1G–1I) and mobility (Figs. 1J and 1K) of OVHM/SK-OV-3 cells in a dose-dependent manner. Additionally, we examined Emd-D's effect on apoptosis using flow cytometric analysis, which revealed that Emd-D effectively induces apoptosis in OVHM and SK-OV-3 cells (Figs. 1L–1N). Collectively, our data suggest that Emd-D exhibits anti-tumor effects on ovarian cancer cells *in vitro*, inhibiting their proliferation, migration, and invasion, while also inducing apoptosis.

3.2. Emd-D induced glycolysis-mediated inhibition of cell growth in vitro

The metabolic requirements of rapidly proliferating tumor cells, including ovarian cancer cells, heavily depend on glycolysis for energy production [25]. Previous research has indicated that emodin, a precursor of Emd-D, exhibits inhibitory effects against glycolysis in renal cancer cells [12]. This study investigated the anticancer properties of Emd-D in ovarian cancer cells through glycolysis inhibition. Initially, we assessed the impact of Emd-D on lactate production, a byproduct of glycolysis. Our results demonstrate that the administration of 100 μmol·L^{-1} of Emd-D led to an

approximately 1.6-fold decrease in lactate content compared to the control group (Fig. 2A). Subsequent investigation of pyruvate levels in the cell supernatant yielded results consistent with reduced lactate production (Fig. 2B). To examine the impact of Emd-D on aerobic glycolysis metabolism, we employed a Seahorse XF analyzer to measure the extracellular acidification rate (a reliable indicator of glycolysis) of OVHM and SK-OV-3 cells following Emd-D treatment. The results indicate that Emd-D treatment impairs the basal and maximal glycolytic capacities of both OVHM and SK-OV-3 cells in a concentration-dependent manner (Figs. 2C and 2D). To further elucidate the effect of Emd-D-mediated glycolytic inhibition on glucose uptake by OVHM cells, we utilized a glucose uptake probe. The data clearly demonstrated that Emd-D dose-dependently decreased the consumption of glucose in OVHM cells (Figs. 2E and 2F). Moreover, Emd-D exhibited the ability to inhibit the expression of glucose transporter 1 (GLUT1) and HK2 in OVHM cells (Figs. 2G–2J), which aligns with the observed reduction in glucose uptake. In conclusion, these findings suggest that Emd-D has the capacity to suppress glycolysis in ovarian cancer cells, consequently inhibiting their proliferation.

3.3. Emd-D as an inhibitor bound to PFKFB4

The analysis of the TCGA database reveals that an upregulation of PFKFB4 expression is elevated in various tumor types, including breast, colorectal, and ovarian cancers (Fig. 3A). The Human Protein Atlas corroborates the presence of PFKFB4 in human ovarian cancer tissues (Fig. 3B). Notably, analysis of samples GSE14764 and GSE26193 from the GEO database revealed a correlation between increased PFKFB4 expression and decreased patient survival time in ovarian cancer, as illustrated in Fig. 3C. To elucidate the molecular interaction between Emd-D and PFKFB4, molecular docking was performed. The docking results (Fig. 3D) indicated a maximum binding affinity of -8.9 kcal·mol^{-1} between Emd-D and PFKFB4. Emd-D adopted a compact conformation while binding to the hydrophobic pocket of PFKFB4, surrounded by residues including Ala-48, Ile-54, Val-163, Val-171, Ile-217, Val-220, Leu-241, Ile-244, and Val-246, forming a strong hydrophobic interaction. Detailed analysis revealed that the anthraquinone scaffold of Emd-D engaged in CH-π interaction with the Tyr-53 residue. Notably, three hydrogen bond interactions were observed between Emd-D and Gly-50 (bond length: 2.3 Å), Asn-167 (bond length:2.0 Å), and Tyr-427 (bond length: 2.7 Å), representing critical interactions between Emd-D and PFKFB4. These interactions facilitated the anchoring of Emd-D within the PFKFB4 binding site. To validate the binding of Emd-D to PFKFB4, total protein extracted from OVHM cells was co-incubated with Emd-D at a dose of 30 μmol·L^{-1}, followed by Pronase E-mediated stabilization assays to assess drug-target binding. Our results indicated that Emd-D administration signific-

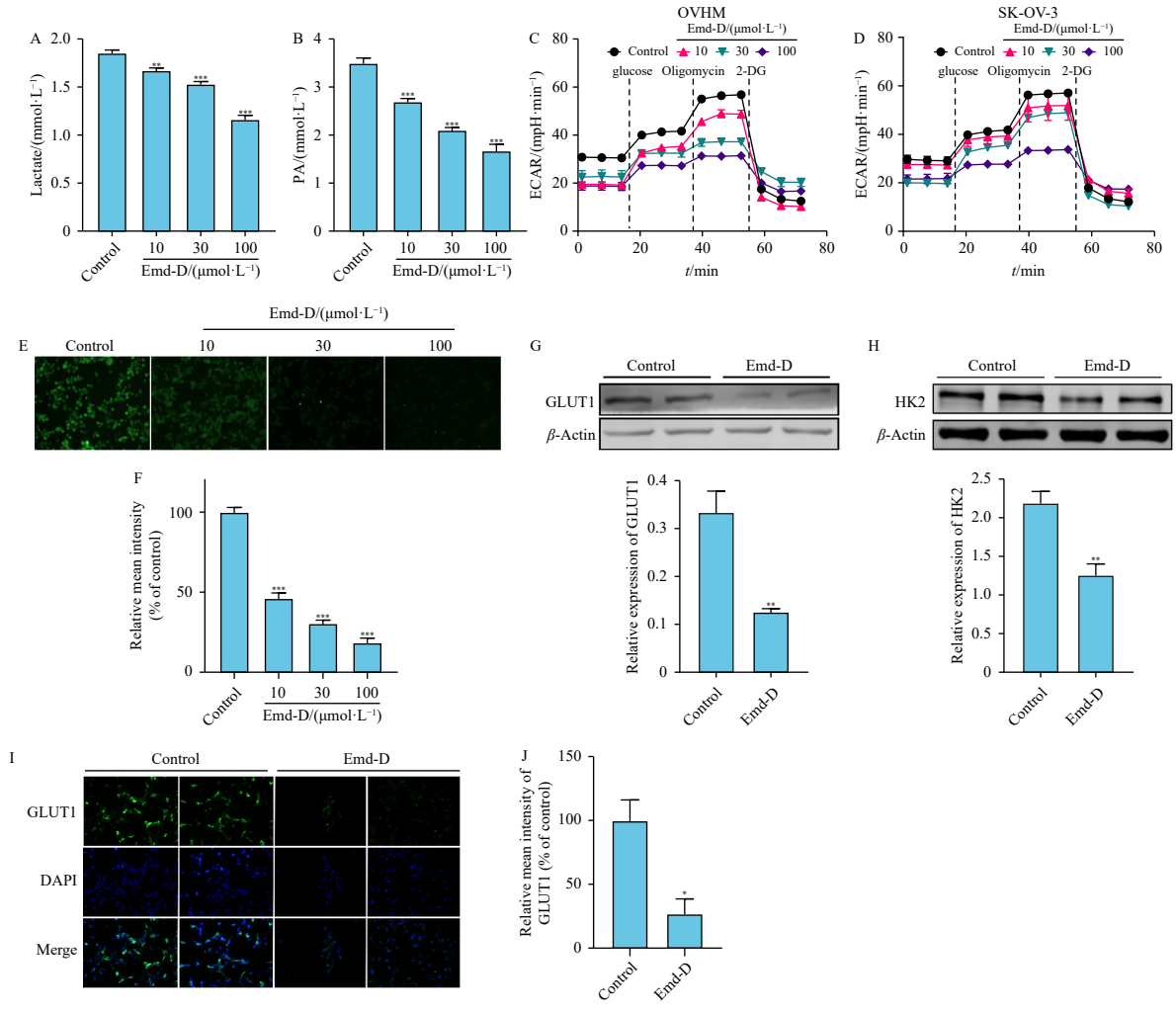

Fig. 2 Emd-D induces glycolysis-mediated inhibition of cell growth in OVHM cells (A) Inhibition of lactate production in OVHM cells by Emd-D. (B) Inhibition of pyruvate production in the supernatant of OVHM cells treated with Emd-D. (C–D) The extracellular acidification rate (ECAR) of OVHM and SK-OV-3 cells under different concentrations of Emd-D treatment was evaluated, and the results are presented as mean ± SEM (n = 5; biological replicates). (E–F) Dose-dependent decrease in glucose consumption by OVHM cells following Emd-D treatment. (G) Inhibition of GLUT1 expression in OVHM cells by Emd-D. (H) Inhibition of HK2 expression in OVHM cells by Emd-D. (I–J) Immunofluorescence analysis of the effect of Emd-D on levels of GLUT1 expression in OVHM cells. All data are shown as the mean ± SEM (n = 4). $^{*}P < 0.05$, $^{**}P < 0.01$, and $^{***}P < 0.001$ *vs* control.

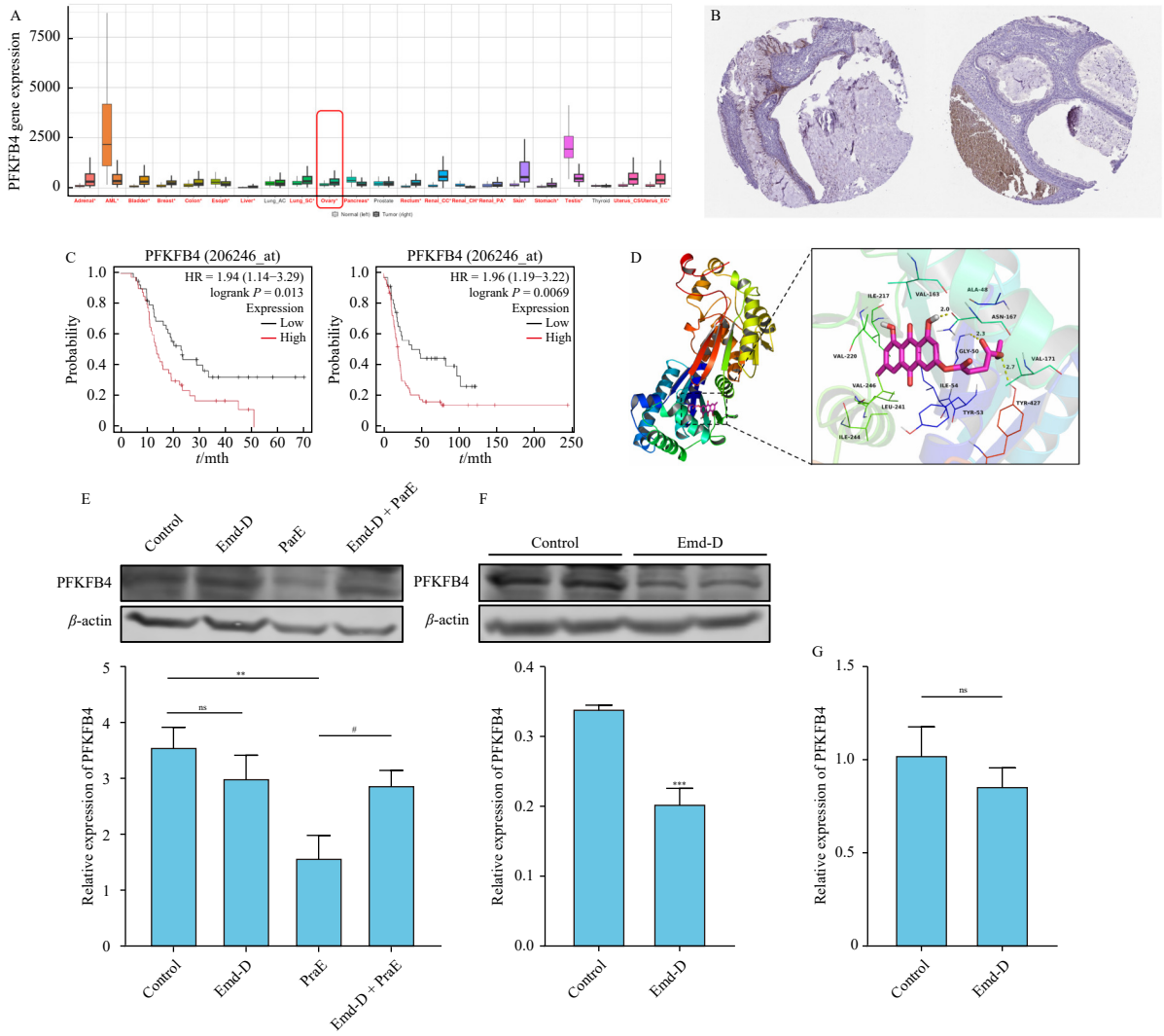

Fig. 3 Binding of Emd-D to PFKFB4 serves as an inhibitor. (A) Analysis based on the TCGA dataset reveals significant upregulation of PFKFB4 expression in ovarian cancer (https://tnmplot.com/). (B) Immunohistochemical analysis conducted at the Proteinatlas website demonstrated the expression of PFKFB4 in ovarian cancer tissues (https://www.proteinatlas.org). (C) Analysis of the GSE14764 (left) and GSE26193 (right) datasets using the kmplot website revealed a significant correlation between high expression of PFKFB4 in ovarian cancer patients and shorter overall survival (https://kmplot.com/). (D) Emd-D was successfully docked into the binding site of PFKFB4, as observed from both total and detailed views. (E) The addition of Emd-D to extracted total cellular protein inhibited the ability of PraE to degrade PFKFB4. Representative plots depict the protein levels of PFKFB4 in the presence and absence of Emd-D and PraE. (F) Representative gel electrophoresis graph showed a reduction in the protein level of PFKFB4 after treating ovarian cancer cells with 30 μmol·L^{-1} Emd-D for 24 h. (G) The mRNA level of *PFKFB4* in OVHM cells remained unaffected in the presence of Emd-D. All data are shown as the mean ± SEM (n = 4). $^{*}P < 0.05$, $^{**}P < 0.01$ *vs* control; $^{\#}P < 0.0.5$ *vs* PraE.

antly enhanced PFKFB4 stability and reduced its vulnerability to proteolytic degradation (Fig. 3E). Moreover, exposing OVHM cells to Emd-D for 24 h resulted in a marked decrease in PFKFB4 protein expression levels (Fig. 3F). Notably, this effect occurred without any apparent change in corresponding mRNA levels, as shown in Fig. 3G. These findings provide a plausible explanation for the interaction between Emd-D and PFKFB4, offering valuable insights for the development of PFKFB4 inhibitors.

3.4. Emd-D inhibited OVHM cell growth via PFKFB4-dependent glycolysis

To examine the dependency of Emd-D's inhibitory effect on ovarian cancer on PFKFB4, we conducted plasmid transfection experiments in OVHM cells. Subsequently, we analyzed the impact of Emd-D on OVHM cells overexpressing PFKFB4. Our results revealed that despite a 1.5-fold increase in PFKFB4 with the treatment of plasmid transfection, Emd-D effectively reduced PFKFB4 expression, as confirmed through Western blot and immunofluorescence staining analyses (Figs. 4A–4C). Notably, our observations indicated that Emd-D treatment reversed the enhanced proliferation, cell viability, invasiveness, and migration potential of PFKFB4-overexpressing OVHM cells (Figs. 4D–4J). These findings suggest that Emd-D exhibits an anti-ovarian cancer effect by inhibiting PFKFB4 expression.

Furthermore, the impact of PFKFB4 overexpression on glycolytic activity in OVHM cells was assessed by evaluating intracellular lactate, pyruvate, and glucose levels. Notably, our findings revealed a significant enhancement in glycolytic activity upon PFKFB4 overexpression in OVHM cells (Figs. 5A–5D). However, it is important to note that even with PFKFB4 overexpression, Emd-D treatment still exerted a suppressive effect on lactate and pyruvate release, as well as glucose uptake in OVHM cells (Figs. 5A–5D). Interestingly, the overexpression of PFKFB4 further counteracted the decrease in GLUT1 and HK2 expression induced by Emd-D (Figs. 5E–5H). In summary, these results indicate that the inhibitory impact of Emd-D on the growth of OVHM cells is partially regulated by PFKFB4-mediated glycolysis.

3.5. Emd-D regulated PFKFB4-mediated apoptosis in OVHM Cells

PFKFB4, a kinase enzyme involved in glucose metabolism, has been shown to play a crucial role in catalyzing various bio-

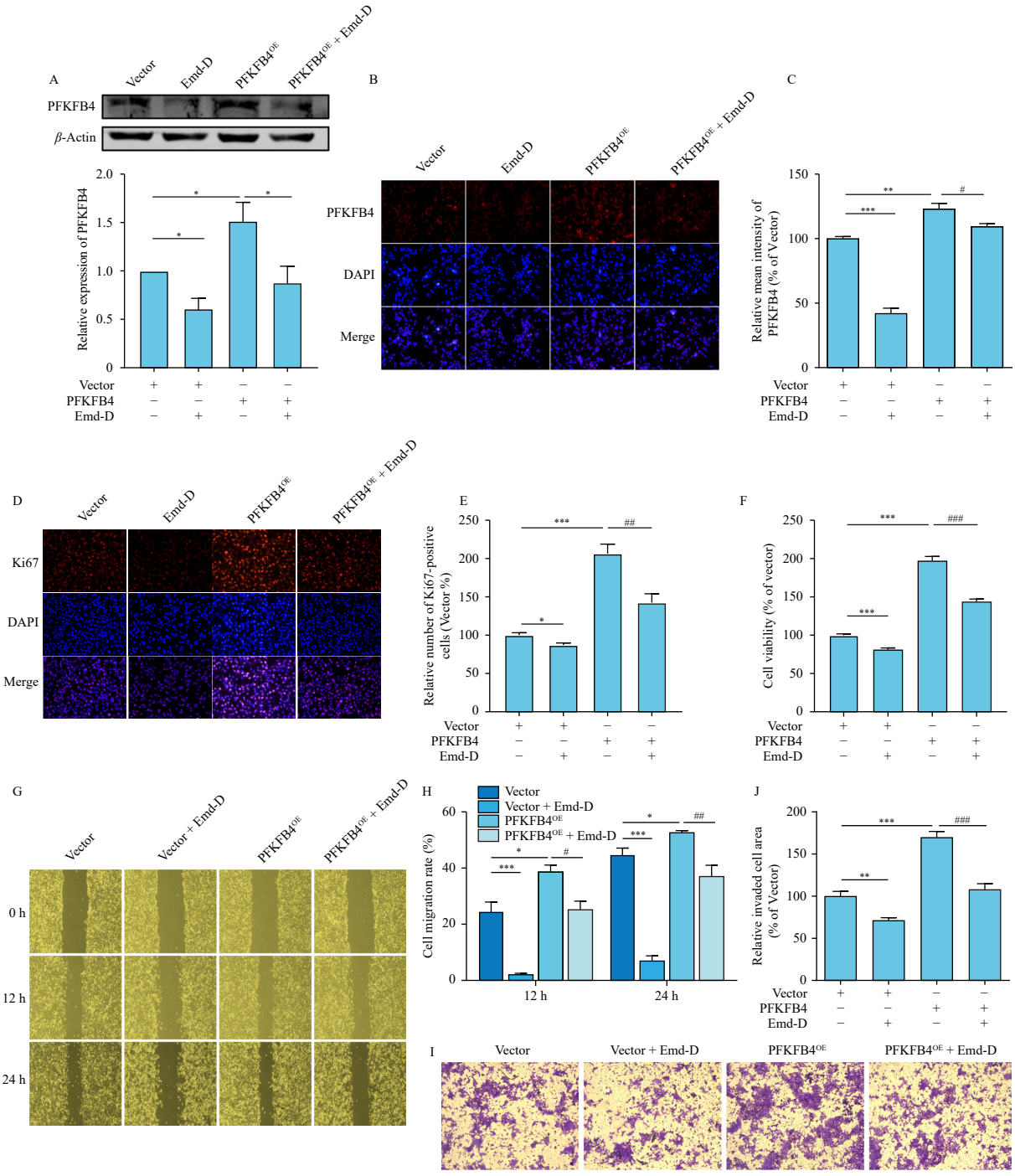

Fig. 4 Overexpression of PFKFB4 reverses Emd-D's inhibition of proliferation and metastasis in OVHM cells. (A) Emd-D maintained its ability to inhibit PFKFB4 expression even after the overexpression of PFKFB4 in OVHM cells. Representative graphs depict the protein levels of PFKFB4. (B–C) Immunofluorescence staining demonstrated that Emd-D effectively suppressed the expression of PFKFB4 in OVHM cells. (D–E) Following PFKFB4 overexpression and 24-h Emd-D treatment, the number of Ki67 positive cells was lower than that of the PFKFB4 overexpression group. (F) Following PFKFB4 overexpression and 24-h Emd-D treatment, cell viability decreased compared with the PFKFB4 overexpression group. (G–H) After 12 and 24 h of PFKFB4 overexpression and Emd-D treatment, cell migration was significantly inhibited compared with the PFKFB4 overexpression group. (I–J) Following PFKFB4 overexpression and Emd-D treatment, cell invasion was significantly inhibited compared with the PFKFB4 overexpression group. All data are shown as the mean ± SEM ($n = 4$). $^{*}P < 0.05$, $^{**}P < 0.01$, and $^{***}P < 0.001$ *vs* Vector; $^{\#}P < 0.05$, $^{\#\#}P < 0.01$, and $^{\#\#\#}P < 0.001$ *vs* PFKFB4.

chemical reactions. Research has indicated its involvement in apoptosis regulation, including autophagy processes [26, 27]. To elucidate the mechanism by which Emd-D induces apoptosis in ovarian cancer cells, this study conducted a comprehensive investigation into its interaction with downstream proteins of PFKFB4. Among these proteins, SRC-3, known to promote ovarian cancer progression and associated with unfavorable prognostic factors, recurrence, and metastasis [28, 29], is phosphorylated by PFKFB4 at the Ser857 site [30]. Immunoblotting analysis revealed that Emd-D inhibited the phosphorylation and activity of SRC-3 (Figs. 6A and 6B). After phosphorylation, SRC-3 translocates to the nucleus where it interacts with ATF-4, initiating transcriptional processes that promote cell proliferation [31]. The results demonstrated that Emd-D treatment led to a reduction in ATF-4 expression levels, indicating that this compound can inhibit tumor cell transcription and propagation (Fig. 6C). Additionally, our data revealed that Emd-D downregulated the expression of ASNS (Fig. 6D), an enzyme responsible for converting aspartate and glutamine into asparagine and glutamate, respectively, in an ATF-4-mediated physiological process that provides essential energy for

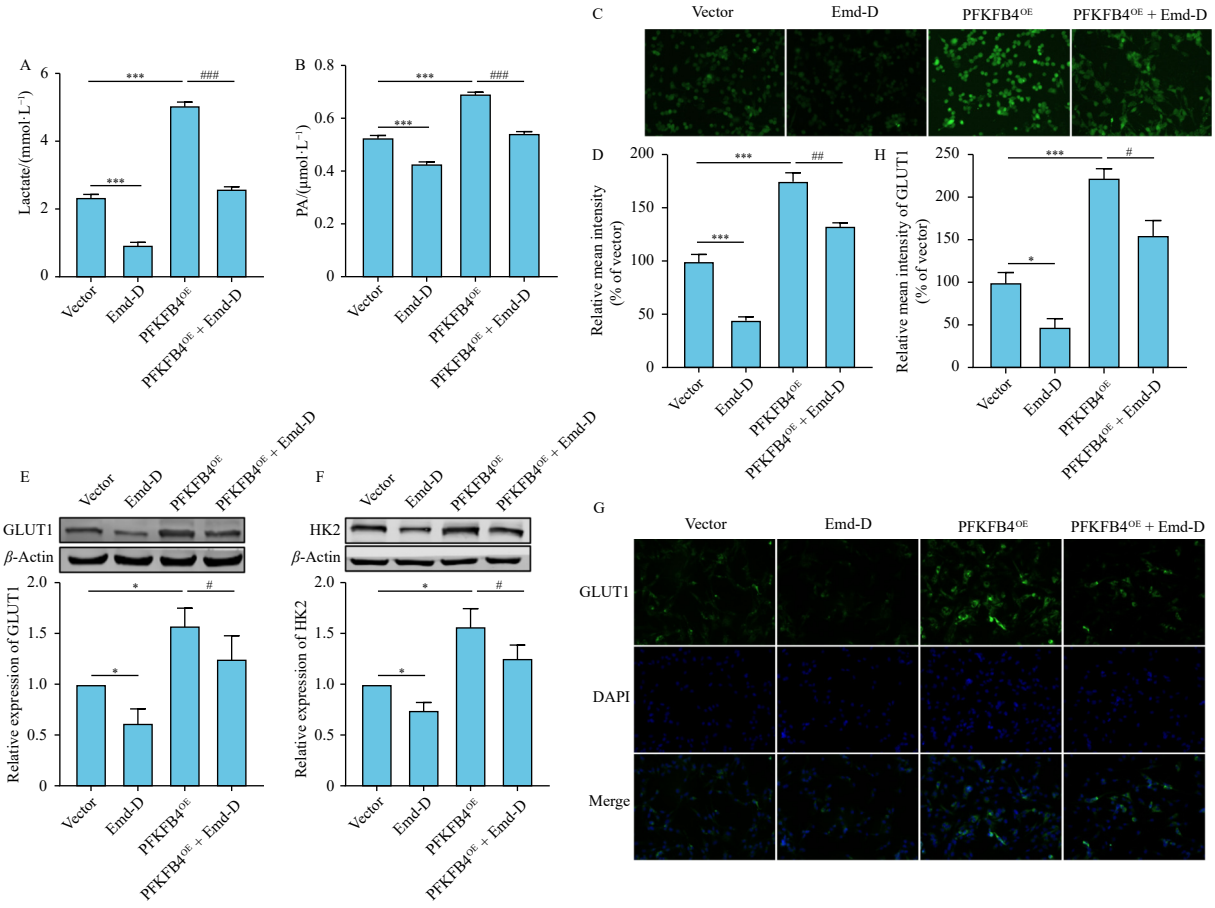

Fig. 5 Overexpression of PFKFB4 negates Emd-D's inhibition of glycolysis in OVHM cells *in vitro*. After transfection of ovarian cancer cells with empty plasmids or PFKFB4 plasmids: (A) The production of lactate, (B) The production of PA, (C–D) Glucose uptake capacity, and protein levels of GLUT1(E), HK2 (F), were all decreased by Emd-D compared with the PFKFB4 overexpression group. (G–H) Immunofluorescence staining demonstrated that the inhibitory effect of Emd-D on GLUT1 expression was abolished by the overexpression of PFKFB4, leading to a decrease in GLUT1 fluorescence level. All data are shown as the mean ± SEM (n = 4). $^{*}P < 0.05$, $^{**}P < 0.01$, and $^{***}P < 0.001$ *vs* Vector; $^{\#}P < 0.05$, $^{\#\#}P < 0.01$, and $^{\#\#\#}P < 0.001$ *vs* PFKFB4.

cells [32]. The role of ASNS in modulating the mTORC1 signaling pathway, which is highly activated in many tumors, promoting tumor metastasis and inhibiting apoptosis, is well-established. Emd-D was observed to reduce the phosphorylation of S6, a readout of mTORC1 activity, and decrease the expression of Bcl-2 (Figs. 6E and 6F), a protein downstream of mTORC1 that promotes cell proliferation [33, 34]. While the expression of the apoptosis-associated protein Bax remained unchanged, the ratio of Bax/Bcl-2 increased (Fig. 6F), suggesting that Emd-D induces apoptosis in ovarian cancer cells through the PFKFB4/SRC-3/ATF-4/mTORC1 signaling axis.

3.6. Emd-D inhibited the growth of ovarian cancer xenograft tumors

To examine the efficacy of Emd-D in inhibiting ovarian cancer progression *in vivo*, we established an ovarian cancer xenograft tumor model by subcutaneously injecting OVHM cells into BALB/c mice. The mice received intraperitoneal DOX twice weekly for a total of 7 administrations, while Emd-D was administered orally once daily for 21 days (Fig. 7A). Tumor growth curves demonstrated that treatment with DOX or Emd-D at doses of 20, 60, and 180 mg·kg^{-1} effectively inhibited tumor development (Fig. 7B). After three weeks of treatment, tumor tissues were excised, and tumor volume and weight were measured and documented (Fig. 7C). As shown in the figure, Emd-D at doses of 60 and 180 mg·kg^{-1} significantly reduced tumor volume and weight (Figs. 7D and 7E). The inhibitory effect of 60 mg·kg^{-1} Emd-D was comparable to that of the positive control drug DOX. Our investigation using TUNEL staining revealed that Emd-D treatment significantly increased the proportion of apoptotic cells in ovarian cancer tissue (Figs. 7F and 7G). Additionally, we observed a marked reduction in the proportion of Ki-67 positive cells in the tumor tissue following Emd-D treatment, suggesting a potential inhibitory effect on cellular proliferation (Figs. 7H and 7I). These findings indicate that Emd-D has the potential to suppress the growth of ovarian xenograft tumors.

3.7. Emd-D inhibited ovarian cancer progression via PFKFB4-dependent glycolysis and apoptosis

To assess the impact of Emd-D on PFKFB4-mediated glycolysis and its subsequent effects on ovarian cancer growth *in vivo*, we investigated PFKFB4 levels in a xenograft tumor model. Our findings reveal a significant decrease in PFKFB4 levels within tumor tissues following Emd-D treatment (Figs. 7J–7L). Moreover, the reduction of lactate (Fig. 8A) and pyruvate (Fig. 8B) levels in tumor tissues provides further evidence of Emd-D's glycolysis-inhibiting capacity in ovarian cancer cells. Notably, protein levels of GLUT1 and HK2 (Figs. 8C–8F), both closely associated with glycolysis, were significantly reduced in Emd-D-treated.

To further elucidate the mechanistic underpinnings of Emd-D-induced apoptosis in ovarian cancer cells, we conducted Western blot assays on ovarian cancer tissues. Our findings provide compelling evidence that Emd-D treatment significantly decreases the expression levels of SRC-3, p-SRC-3, ATF-4, ASNS, p-S6, and Bcl-2. Simultaneously, it reduces the Bcl-2/Bax ratio, consistent with our observations from cellular assays (Figs. 8G–8L). These res-

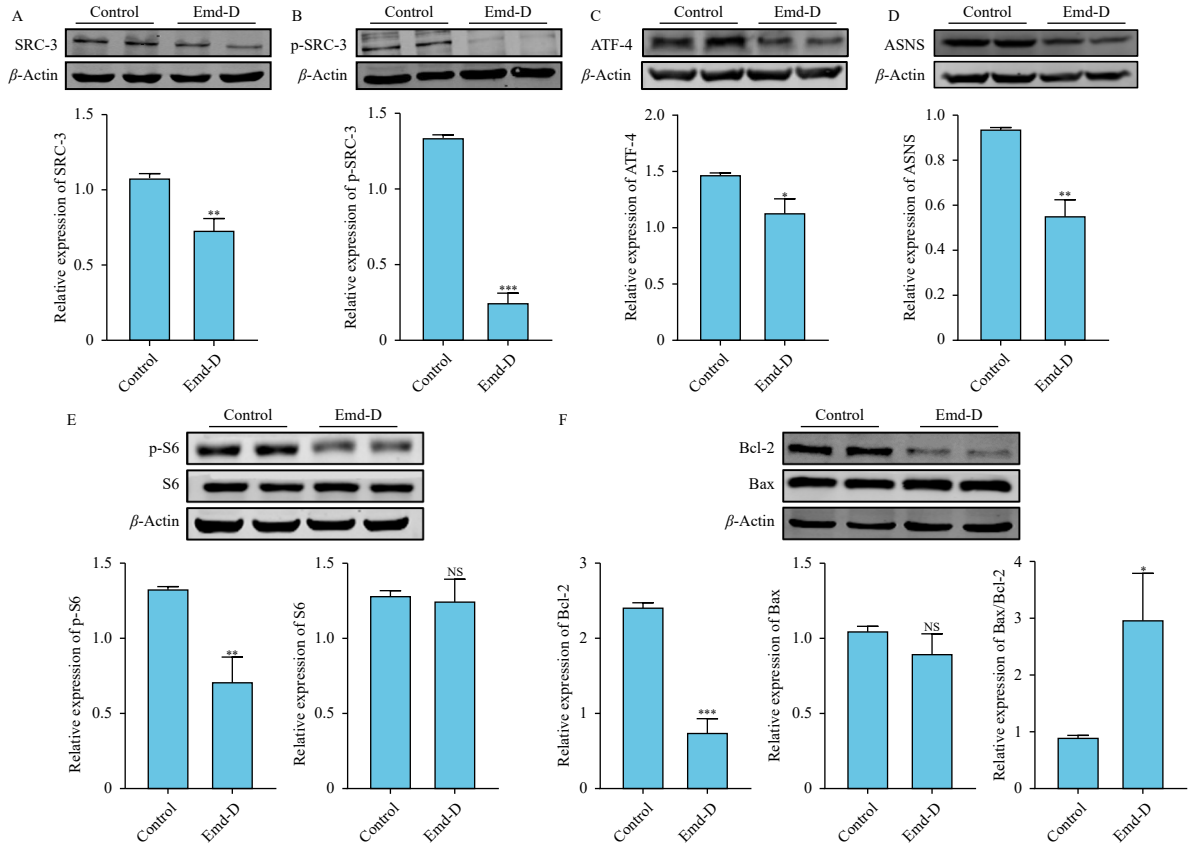

Fig. 6 Emd-D regulated PFKFB4-mediated SRC3/ATF-4/mTORC1 pathway *in vitro* Following a 24-h treatment with Emd-D, there was a prominent suppression in the expression of SRC-3 (A), p-SRC-3 (B), ATF-4 (C), ASNS (D), p-S6 (E) and Bcl-2 (F) in OVHM cells. Despite this, the expression of Bax remained unaltered, leading to an increase in the Bax/Bcl-2 ratio (F). All data are shown as the mean ± SEM (n = 4). $^{*}P < 0.05$, $^{**}P < 0.01$, and $^{***}P < 0.001$ *vs* control.

ults demonstrate that Emd-D inhibits ovarian cancer progression by modulating PFKFB4-mediated glycolysis and apoptosis *in vitro* and *in vivo*.

4. Discussion

Ovarian cancer is typically diagnosed at an advanced stage, limiting available treatment options. Current interventions, including surgery and chemotherapy, often result in adverse side effects and increased recurrence rates [24, 35]. While targeted drugs and immunotherapies exist, they have not extended PFS or OS for ovarian cancer patients [36]. Consequently, the development of alternative therapies has become imperative. Traditional Chinese medicine and its constituent monomers have been extensively utilized in tumor management, making them valuable sources of chemotherapeutic agents [13]. Emd-D, a novel drug developed by our team, represents a significant advancement from emodin through the modification of natural drugs to enhance therapeutic efficacy and reduce toxicity. Based on tPSA, LogP, and Gibbs free energy values calculated using Lipinski's rule, Emd-D demonstrates superior drug formability and higher bioavailability compared to emodin [20]. Despite these advancements, the efficacy of Emd-D in treating ovarian cancer remains uncertain. In this study, we present the first evidence of Emd-D's ability to induce apoptosis and inhibit glycolysis in ovarian cancer cells. In conclusion, this study presents compelling evidence supporting the potential clinical applicability of Emd-D as a promising chemotherapeutic agent for ovarian cancer treatment. The observed therapeutic effects of Emd-D, including significant tumor regression in animal models, demonstrate its efficacy and warrant further investigation.

Utilizing an ovarian cancer xenograft tumor model, we demonstrated that Emd-D has the ability to inhibit tumor growth, reduce tumor size, and decrease tumor weight compared to the model group. Our findings suggest that Emd-D may serve as a potential alternative to current chemotherapeutic agents due to its lower toxicity profile, higher safety index, and inherent capacity to impede the progression of ovarian cancer. Taken together, these data indicate that Emd-D represents a promising therapeutic candidate for ovarian cancer treatment, given its superior efficacy and safety profile compared to current chemotherapeutic agents such as DOX. The development and clinical translation of Emd-D could potentially offer patients a more efficacious and safer treatment option for ovarian cancer. Further studies are needed to fully characterize the mechanisms underlying the anticancer properties of Emd-D and determine its clinical potential.

Tumor cells exhibit an increased demand for energy due to their rapid proliferation rate, consequently reprogramming glucose metabolism *via* the Warburg effect to provide a substantial energy source [6]. Targeting glucose metabolism in tumor cells has emerged as a promising antitumor therapy. While previous studies have identified emodin as a blood glucose regulator [37], the role of Emd-D in glucose metabolism regulation remains unclear. Therefore, we hypothesized that Emd-D may suppress glycolysis in ovarian cancer. Our findings demonstrate that incubation of OVHM cells with Emd-D inhibits the accumulation of extracellular pyruvate and lactate, while also reducing intracellular glucose content. Furthermore, Emd-D treatment decreased the expressions of GLUT1 and HK2, which are critical components of glucose metabolism. These results support the hypothesis that Emd-D may serve as an inhibitor of glycolysis in ovarian cancer, suggesting its potential as a therapeutic agent for ovarian cancer treatment by targeting glucose metabolism.

PFKFB4, a crucial protein regulating key metabolic pathways in tumor cells, including glycolysis, autophagy, and apoptosis, has emerged as a promising therapeutic target for cancer treatment.

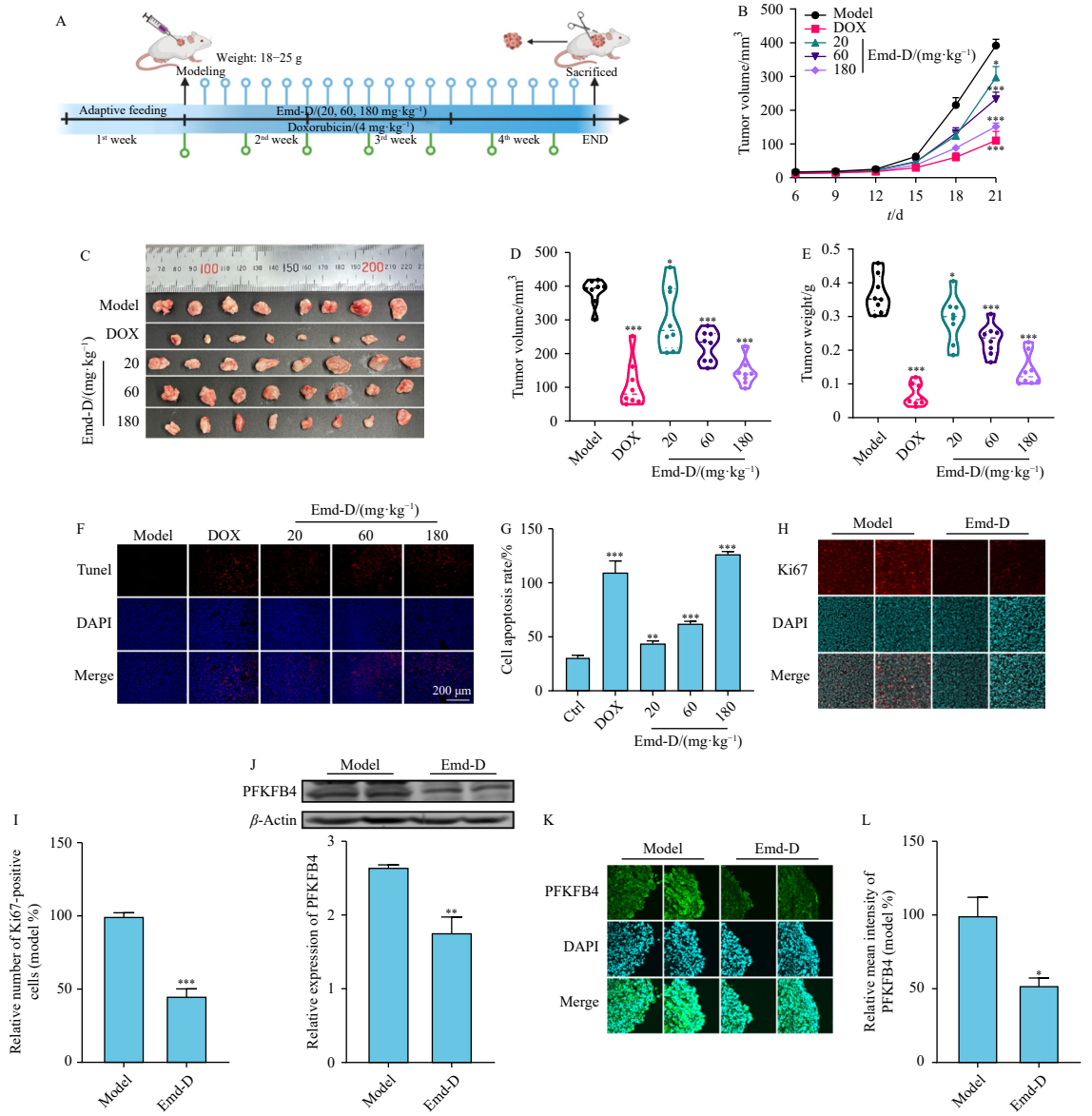

Fig. 7 Emd-D inhibited the growth of ovarian cancer xenograft tumors. (A) Schematic illustration of the timeline for tumor induction and treatment in mice. (B) The tumor growth curve was evaluated after ovarian cancer model establishment, where each group was administered drinking water, DOX, or varied amounts of Emd-D. Tumor size was measured at 3 d intervals, and tumor volume was calculated accordingly. Growth curves were then plotted based on these measurements. (C) Representative image of tumor tissue. (D–E) A graph showcasing statistical analysis of tumor volumes (D) and weights (E) are provided. (n = 8). (F–G) Representative and statistical graphs of TUNEL staining. Emd-D treatment results in an increase in the proportion of apoptotic cells in ovarian cancer tissue. (H–I) Staining of Ki67 indicated that Emd-D resulted in a reduction in the proportion of Ki67-positive cells in tumor tissues. (J) Detection of PFKFB4 protein levels in tumor tissues were evaluated *via* Western blot analysis. (K–L) Immunofluorescence assessment of the influence of Emd-D on PFKFB4 expression levels in tumor tissues. All data are shown as the mean ± SEM (n = 4). $^{*}P < 0.05$, $^{**}P < 0.01$, and $^{***}P < 0.001$ *vs* model.

Its involvement in regulating cell death, proliferation, and metastasis underscores its significance. Bruceine A has been identified as a PFKFB4 inhibitor, leading to reduced glycolysis rates and suppressed pancreatic cancer progression [38]. Notably, PFKFB4 expression levels are significantly elevated in ovarian cancer tissues compared to paraneoplastic tissues. Based on our findings that Emd-D could inhibit glycolysis in ovarian cancer, we hypothesized that Emd-D might target PFKFB4 and regulate proliferation of ovarian cancer cells. Our experimental results, utilizing molecular docking and drug target binding stability assays, confirmed that Emd-D can indeed bind to PFKFB4 and inhibit its expression. Notably, the overexpression of PFKFB4 in ovarian cancer cells mitigates the inhibitory effects of Emd-D on tumor proliferation and metastasis. These findings suggest that Emd-D could potentially serve as a therapeutic agent for treating ovarian cancer by interfering with PFKFB4-mediated pathways.

Phosphorylation of the Ser857 site of SRC-3 by PFKFB4 results in the constitutive activation of SRC-3, thereby enhancing transcriptional activity, glucose flux, and targeted gene synthesis [30]. However, these effects may inadvertently contribute to the promotion of various tumors. In ER-positive breast cancer cells, the interaction between SRC-3 and PFKFB4, as well as PFKFB3, facilitates the progression of cancer stem cell characterization and circulating tumor cell development, ultimately leading to breast cancer recurrence and metastasis [39]. The research findings demonstrate that Emd-D intervention can effectively reduce the total and phosphorylation level of SRC-3, thus confirming its inhibitory effect on PFKFB4-mediated SRC-3 activation.

Notably, phosphorylated SRC-3 can translocate to the nucleus and interact with ATF-4, facilitating the activation of transcription programs such as ASNS and mTORC1. ASNS is responsible for asparagine synthesis, while mTORC1 plays a crucial role in various metabolic processes, including glucose and lipid metabolism, nucleotide synthesis, and protein synthesis. Furthermore, mTORC1's role in tumor cells is multifaceted, influencing glucose transport and the activities of metabolic enzymes such as HK2,

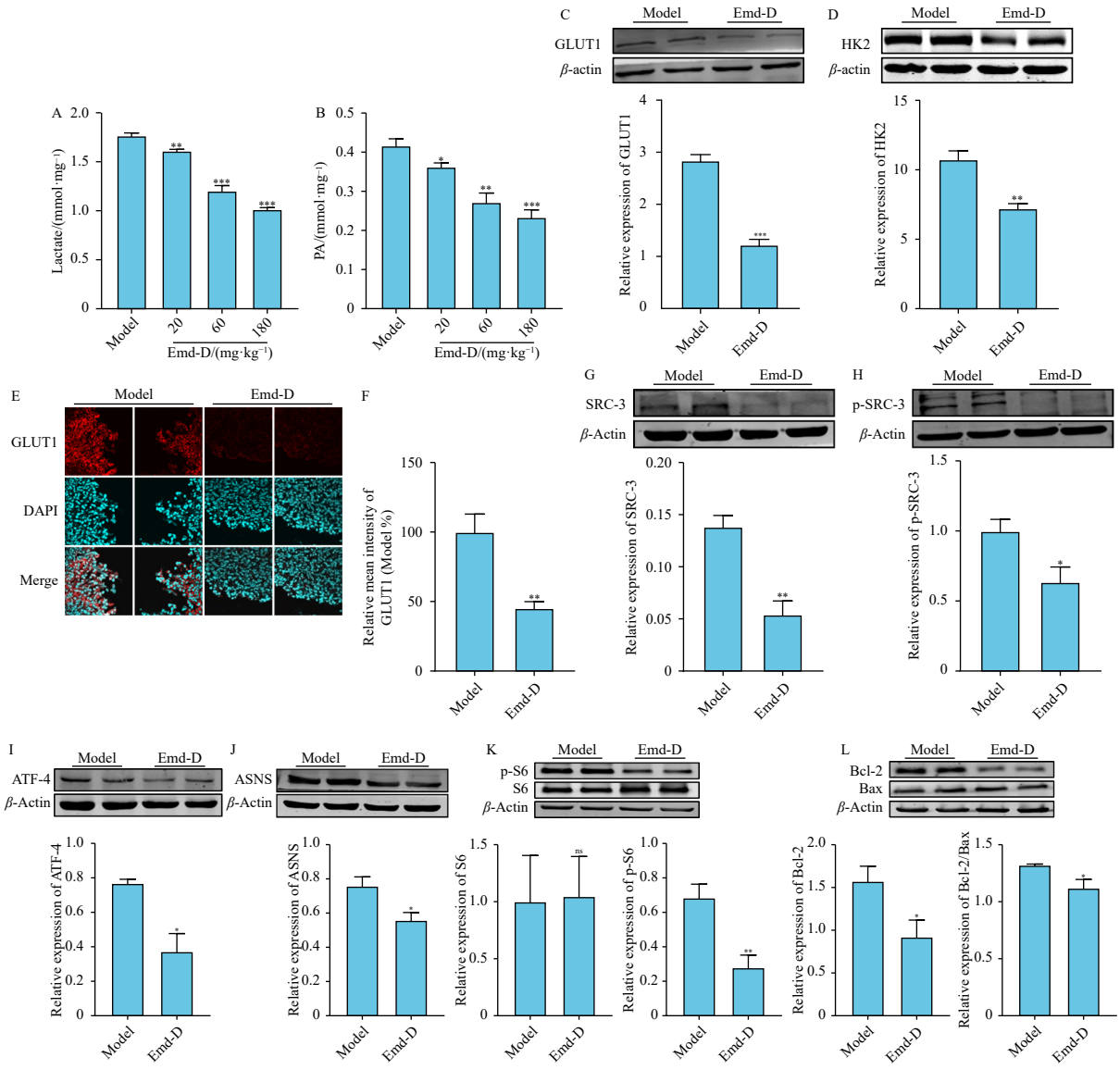

Fig. 8 Emd-D inhibited the PFKFB4/SRC-3/ATF-4 signaling pathway *in vivo*. (A) Emd-D demonstrated inhibition of lactate production in tumor tissues. (B) Emd-D suppressed pyruvate production in tumor tissues. (C) GLUT1 expression was inhibited in tumor tissues following treatment with Emd-D. (D) HK2 expression was inhibited in tumor tissues following treatment with Emd-D. (E–F) Immunofluorescence showed the inhibition of GLUT1 expression in tumor tissues by Emd-D. (G) SRC-3 total protein expression, (H) extent of its phosphorylation, (I) ATF-4 protein abundance, (J) ASNS protein levels, (K) S6 and p-S6 protein expression levels and (L) Bcl-2 and Bax protein amounts in tumor tissues were evaluated *via* Western blot analysis. All data are shown as the mean ± SEM ($n = 4$). $^{*}P < 0.05$, $^{**}P < 0.01$, and $^{***}P < 0.001$ *vs* model.

PFK, and PKM via HIF-1α and MYC, resulting in increased glycolysis rates. Consequently, this affects the tricarboxylic acid cycle and ATP synthesis, promoting tumor cell proliferation. Significantly, mTORC1 inhibition has been strongly associated with apoptosis and is increasingly becoming a focus in drug development [32, 33, 40]. The inhibitory effect of Emd-D on ovarian cancer glycolysis and promotion of apoptosis was found to be reflected in mTORC1 inhibition, suggesting that Emd-D exerts a regulatory function in apoptosis and glycolytic processes mediated by PFKFB4, potentially offering therapeutic value for ovarian cancer treatment.

5. Conclusion

In conclusion, this study demonstrates the potential of Emd-D as an anti-ovarian cancer agent through its dual mechanism of action: inhibition of the PFKFB4-dependent glycolysis pathway and induction of apoptosis. These findings establish a robust foundation for further investigation of Emd-D as a promising therapeutic candidate in the treatment of ovarian cancer.

Funding

This research was funded by the Natural Science Foundation of Heilongjiang Province (No. LH2023H012), Postdoctoral Research Initiation Fund (No. LBH-Q20152), and CAMS Innovation Fund for Medical Sciences (CIFMS, 2019-I2M-5-078).

Declaration of competing interest

These authors have no conflict of interest to declare.

References

1 Siegel RL, Miller KD, Jemal A. Cancer statistics, 2020. *CA Cancer J Clin*. 2020;70(1):7-30. https://doi.org/10.3322/caac.21590.
2 Zheng RS, Sun KX, Zhang SW, et al. Report of cancer epidemiology in China, 2015. *Chin J Oncol*. 2019;41(1):19-28.
3 Miller KD, Nogueira L, Mariotto AB, et al. Cancer treatment and survivorship statistics, 2019. *CA Cancer J Clin*. 2019;69(5):363-385. https://doi.org/10.3322/caac.21565.
4 Orr B, Edwards RP. Diagnosis and treatment of ovarian cancer. *Hematol Oncol Clin North Am*. 2018;32(6):943-964. https://doi.org/10.1016/j.hoc.2018.07.010.

5 Pavlova NN, Thompson CB. The emerging hallmarks of cancer metabolism. *Cell Metab*. 2016;23(1):27-47. https://doi.org/10.1016/j.cmet.2015.12.006.
6 Schwartz L, Supuran CT, Alfarouk KO. The warburg effect and the hallmarks of cancer. *Anticancer Agents Med Chem*. 2017;17(2):164-170. https://doi.org/10.2174/1871520616666161031143301.
7 Kobayashi Y, Banno K, Kunitomi H, et al. Warburg effect in Gynecologic cancers. *J Obstet Gynaecol Res*. 2019;45(3):542-548. https://doi.org/10.1111/jog.13867.
8 Floridi A, Paggi MG, Marcante ML, et al. Lonidamine, a selective inhibitor of aerobic glycolysis of murine tumor cells. *J Natl Cancer Inst*. 1981;66(3):497-499.
9 Di Cosimo S, Ferretti G, Papaldo P, et al. Lonidamine: efficacy and safety in clinical trials for the treatment of solid tumors. *Drugs Today (Barc)*. 2003;39(3):157-174. https://doi.org/10.1358/dot.2003.39.3.799451.
10 Pajak B, Siwiak E, Soltyka M, et al. 2-Deoxy-D-glucose and its analogs: from diagnostic to therapeutic agents. *Int J Mol Sci*. 2019;21(1):234. https://doi.org/10.3390/ijms21010234.
11 Woodward GE, Hudson MT. The effect of 2-desoxy-D-glucose on glycolysis and respiration of tumor and normal tissues. *Cancer Res*. 1954;14(8):599-605.
12 Wang KJ, Meng XY, Chen JF, et al. Emodin induced necroptosis and inhibited glycolysis in the renal cancer cells by enhancing ROS. *Oxid Med Cell Longev*. 2021;2021:8840590. https://doi.org/10.1155/2021/8840590.
13 Xiang Y, Guo Z, Zhu P, et al. Traditional Chinese medicine as a cancer treatment: modern perspectives of ancient but advanced science. *Cancer Med*. 2019;8(5):1958-1975. https://doi.org/10.1002/cam4.2108.
14 Monisha BA, Kumar N, Tiku AB. Emodin and its role in chronic diseases. *Adv Exp Med Biol*. 2016;928:47-73. https://doi.org/10.1007/978-3-319-41334-1_3.
15 Ma L, Yang Y, Yin Z, et al. Emodin suppresses the nasopharyngeal carcinoma cells by targeting the chloride channels. *Biomed Pharmacother*. 2017;90:615-625. https://doi.org/10.1016/j.biopha.2017.03.088.
16 Chang X, Zhao J, Tian F, et al. Aloe-emodin suppresses esophageal cancer cell TE1 proliferation by inhibiting AKT and ERK phosphorylation. *Oncol Lett*. 2016;12(3):2232-2238. https://doi.org/10.3892/ol.2016.4910.
17 Chen C, Gao J, Wang TS, et al. NMR-based metabolomic techniques identify the toxicity of emodin in HepG2 cells. *Sci Rep*. 2018;8(1):9379. https://doi.org/10.1038/s41598-018-27359-4.
18 Chang MH, Huang FJ, Chan WH. Emodin induces embryonic toxicity in mouse blastocysts through apoptosis. *Toxicology*. 2012;299(1):25-32. https://doi.org/10.1016/j.tox.2012.05.006.
19 He Q, Liu K, Wang S, et al. Toxicity induced by emodin on zebrafish embryos. *Drug Chem Toxicol*. 2012;35(2):149-154. https://doi.org/10.3109/01480545.2011.589447.
20 Liu X, Han W, An N, et al. Kanglexin protects against cardiac fibrosis and dysfunction in mice by TGF-β1/ERK1/2 noncanonical pathway. *Front Pharmacol*. 2020;11:572637. https://doi.org/10.3389/fphar.2020.572637.
21 Trotto O, Olson AJ. AutoDock Vina: improving the speed and accuracy of docking with a new scoring function, efficient optimization, and multithreading. *J Comput Chem*. 2010;31(2):455-461. https://doi.org/10.1002/jcc.21334.
22 Sanner MF. Python: a programming language for software integration and development. *J Mol Graph Model*. 1999;17(1):57-61.
23 Morris GM, Huey R, Lindstrom W, et al. AutoDock4 and AutoDockTools4: automated docking with selective receptor flexibility. *J Comput Chem*. 2009;30(16):2785-2791. https://doi.org/10.1002/jcc.21256.
24 Wan L, Pantel K, Kang Y. Tumor metastasis: moving new biological insights into the clinic. *Nat Med*. 2013;19(11):1450-1464. https://doi.org/10.1038/nm.3391.
25 Zhang D, Li Y, Yang S, et al. Identification of a glycolysis-related gene signature for survival prediction of ovarian cancer patients. *Cancer Med*. 2021;10(22):8222-8237. https://doi.org/10.1002/cam4.4317.
26 Kotowski K, Rosik J, Machaj F, et al. Role of PFKFB3 and PFKFB4 in cancer: genetic basis, impact on disease development/progression, and potential as therapeutic targets. *Cancers (Basel)*. 2021;13(4):909.
27 Jalal S, Zhang T, Deng J, et al. *β*-Elemene isopropanolamine derivative LXX-8250 induces apoptosis through impairing autophagic flux *via* PFKFB4 repression in melanoma cells. *Front Pharmacol*. 2022;13:900973. https://doi.org/10.3389/fphar.2022.900973.
28 Palmieri C, Gojis O, Rudraraju B, et al. Expression of steroid receptor coactivator 3 in ovarian epithelial cancer is a poor prognostic factor and a marker for platinum resistance. *Br J Cancer*. 2013;108(10):2039-2044. https://doi.org/10.1038/bjc.2013.199.
29 Yoshida H, Liu J, Samuel S, et al. Steroid receptor coactivator-3, a homolog of Taiman that controls cell migration in the Drosophila ovary, regulates migration of human ovarian cancer cells. *Mol Cell Endocrinol*. 2005;245(1-2):77-85. https://doi.org/10.1016/j.mce.2005.10.008.
30 Dasgupta S, Rajapakshe K, Zhu B, et al. Metabolic enzyme PFKFB4 activates transcriptional coactivator SRC-3 to drive breast cancer. *Nature*. 2018;556(7700):249-254. https://doi.org/10.1038/s41586-018-0018-1.
31 Statzer C, Meng J, Venz R, et al. ATF-4 and hydrogen sulfide signalling mediate longevity in response to inhibition of translation or mTORC1. *Nat Commun*. 2022;13(1):967. https://doi.org/10.1038/s41467-022-28599-9.
32 Su N, Kilberg MS. C/EBP homology protein (CHOP) interacts with activating transcription factor 4 (ATF4) and negatively regulates the stress-dependent induction of the asparagine synthetase gene. *J Biol Chem*. 2008;283(50):35106-35117. https://doi.org/10.1074/jbc.M806874200.
33 Kim LC, Cook RS, Chen J. mTORC1 and mTORC2 in cancer and the tumor microenvironment. *Oncogene*. 2017;36(16):2191-2201. https://doi.org/10.1038/onc.2016.363.
34 Vernieri C, Corti F, Nichetti F, et al. Everolimus versus alpelisib in advanced hormone receptor-positive HER2-negative breast cancer: targeting different nodes of the PI3K/AKT/mTORC1 pathway with different clinical implications. *Breast Cancer Res*. 2020;22(1):33. https://doi.org/10.1186/s13058-020-01271-0.
35 Eisenhauer EA. Real-world evidence in the treatment of ovarian cancer. *Ann Oncol*. 2017;28(suppl_8):viii61-viii5. https://doi.org/10.1093/annonc/mdx443.
36 Yang C, Xia BR, Zhang ZC, et al. Immunotherapy for ovarian cancer: adjuvant, combination, and neoadjuvant. *Front Immunol*. 2020;11:577869. https://doi.org/10.3389/fimmu.2020.577869.
37 Cheng L, Zhang S, Shang F, et al. Emodin improves glucose and lipid metabolism disorders in obese mice *via* activating brown adipose tissue and inducing browning of white adipose tissue. *Front Endocrinol (Lausanne)*. 2021;12:618037. https://doi.org/10.3389/fendo.2021.618037.
38 Zhang P, Tao W, Lu C, et al. Bruceine A induces cell growth inhibition and apoptosis through PFKFB4/GSK3β signaling in pancreatic cancer. *Pharmacol Res*. 2021;169:105658. https://doi.org/10.1016/j.phrs.2021.105658.
39 Truong TH, Benner EA, Hagen KM, et al. PELP1/SRC-3-dependent regulation of metabolic PFKFB kinases drives therapy resistant ER^+ breast cancer. *Oncogene*. 2021;40(25):4384-4397. https://doi.org/10.1038/s41388-021-01871-w.
40 Gwinn DM, Lee AG, Briones-Martin-Del-Campo M, et al. Oncogenic KRAS regulates amino acid homeostasis and asparagine biosynthesis *via* ATF4 and alters sensitivity to L-asparaginase. *Cancer Cell*. 2018;33(1):91-107.e6. https://doi.org/10.1016/j.ccell.2017.12.003.